Journal of Power Sources 195 (2010) 6798–6804

Contents lists available at ScienceDirect

Journal of Power Sources

journal homepage: www.elsevier.com/locate/jpowsour

Short communication

Nitrogen plasma-implanted titanium as bipolar plates in polymer electrolyte membrane fuel cells

Kai Feng[a,b], Dixon T.K. Kwok[b], Dongan Liu[c], Zhuguo Li[a], Xun Cai[a,*], Paul K. Chu[b,**]

[a] Shanghai Key Laboratory of Materials Laser Processing and Modification, School of Materials Science and Engineering, Shanghai Jiao Tong University, Dongchuan Road 800#, Minhang, Shanghai 200240, China
[b] Department of Physics and Materials Science, City University of Hong Kong, Tat Chee Avenue, Kowloon, Hong Kong, China
[c] School of Mechanical Engineering, Shanghai Jiao Tong University, Shanghai 200240, China

ARTICLE INFO

Article history:
Received 15 March 2010
Received in revised form 15 April 2010
Accepted 16 April 2010
Available online 22 April 2010

Keywords:
Bipolar plate
Polymer electrolyte membrane fuel cells
Plasma immersion ion implantation
Corrosion resistance
Titanium

ABSTRACT

Nitrogen plasma immersion ion implantation (PIII), a non-line-of-sight surface treatment technique suitable for bipolar plates in polymer electrolyte membrane fuel cells, is conducted at low and high temperature to improve the corrosion resistance and conductivity of titanium sheets. X-ray photoelectron spectroscopy (XPS) shows that high-temperature (HT) nitrogen PIII produces a thick oxy-nitride layer on the titanium surface. This layer which provides good corrosion resistance and high electrical conductivity as verified by electrochemical tests, inductively coupled plasma optical emission spectroscopy, and interfacial contact resistance (ICR) measurements renders the materials suitable for polymer electrolyte membrane fuel cells. In comparison, the low-temperature (LT) PIII titanium sample exhibits poorer corrosion resistance and electrical conductivity than the untreated titanium control.

1. Introduction

The polymer electrolyte membrane fuel cell (PEMFC) is promising in transportation applications and portable devices due to its high efficiency, cleanliness, and low operating temperature (70–90 °C) [1–3]. The bipolar plate which is the key component in the PEMFC performs multiple functions [4–6]. For instance, it separates the individual fuel cells, conducts the electrons to the adjoining cells as a current collector, supports the membrane electrode assembly (MEA), supplies the reactive gas, hydrogen, to the anode and oxygen to the cathode via flow channels, and removes the heat and reaction products (water). The requirements for the bipolar plate include high electrical conductivity, good corrosion resistance, high gas impermeability, and good mechanical performance [7,8].

Metallic materials are used in the bipolar plate because of their good mechanical strength, high electrical conductivity, high gas impermeability, low cost, and ease of manufacturing compared to the conventional graphite materials [9–13]. However, a metallic bipolar plate is plagued by two problems that can significantly degrade the PEMFC stack performance. The first one is surface corrosion which leads to release of metal ions contaminating the electrolyte membrane and poisoning the electrode catalysts [14]. The second one is the passive film on the metal surface which can increase the interfacial contact resistance between the bipolar plate and adjacent carbon paper by several orders of magnitude [15]. Therefore, various types of coatings have been investigated as possible bipolar plate materials, especially from the perspective of corrosion prevention [9,15–20]. Among them, titanium nitride has been extensively investigated due to its good corrosion resistance, low interfacial contact resistance, and easy fabrication. Li et al. [6] deposited a titanium nitride coating on the 316L stainless steel bipolar plate by physical vapor deposition (PVD) to protect the substrate from the corrosive electrolyte in the PEMFC. Wang and Northwood [21] evaluated the corrosion resistance of TiN coated 316L stainless steel and demonstrated significantly reduced corrosion current. The potentiostatic test results showed that the current density in the simulated cathode environment increased by threefold due to pitting corrosion. In fact, the presence of defects in the coating such as pinholes and macroparticles that are common to PVD can adversely affect the corrosion resistance [22,23]. Kim et al. [24] deposited TiN_xO_y films on stainless steel 316L by inductively coupled plasma assisted sputtering and found that when a small amount of oxygen was incorporated into the TiN films, the corrosion resistance and conductivity could be improved.

Titanium is one of the potential bipolar plate materials due to its good corrosion resistance in highly acidic and humid conditions even at high positive overpotentials [25] and low density. It is especially suitable for bipolar plates in micro-PEM fuel cells in portable

* Corresponding author. Tel.: +86 21 54748940; fax: +86 21 62182903.
** Corresponding author. Tel.: +852 34427724; fax: +852 27889549.
E-mail addresses: xcai@sjtu.edu.cn (X. Cai), paul.chu@cityu.edu.hk (P.K. Chu).

0378-7753/$ – see front matter © 2010 Elsevier B.V. All rights reserved.
doi:10.1016/j.jpowsour.2010.04.053

devices which can command a higher price compared to PEM fuel cells found in automobiles because of added values such as relatively low density and high strength. However, surface modification is necessary to improve the corrosion resistance and contact resistance before the materials can be used in bipolar plates. Hodgson et al. [26] studied the performance of FC5 coated titanium as bipolar plates and suggested that coated titanium could be employed to produce fuel cells with very high volumetric and gravimetric power densities suitable for portable applications. Wang et al. [27] evaluated two different surface modified materials, iridium oxide (IrO_2) and platinum and observed that the cell performance was close to that of the PEM fuel cells using graphite bipolar plates. Show et al. [18] prepared amorphous carbon films on titanium bipolar plates at various temperature and their results showed that the a-C film prepared at 600 °C possessed a low resistivity of 10^{-3} Ω-cm and the fuel cell comprising this bipolar plates had an output power that was 1.4 times higher than that of a fuel cell containing a bare Ti bipolar plate. Jung et al. [25] indicated that a 1 μm thick gold coating on the titanium bipolar plate led to stable performance and was very effective in preventing oxidation of titanium during operation of the PEMFC. Liu et al. [12] carried out plasma nitriding at 1173 K for 4 h on a titanium sheet and revealed that both the electrical conductivity and corrosion resistance after plasma nitriding did not reach the levels of graphite.

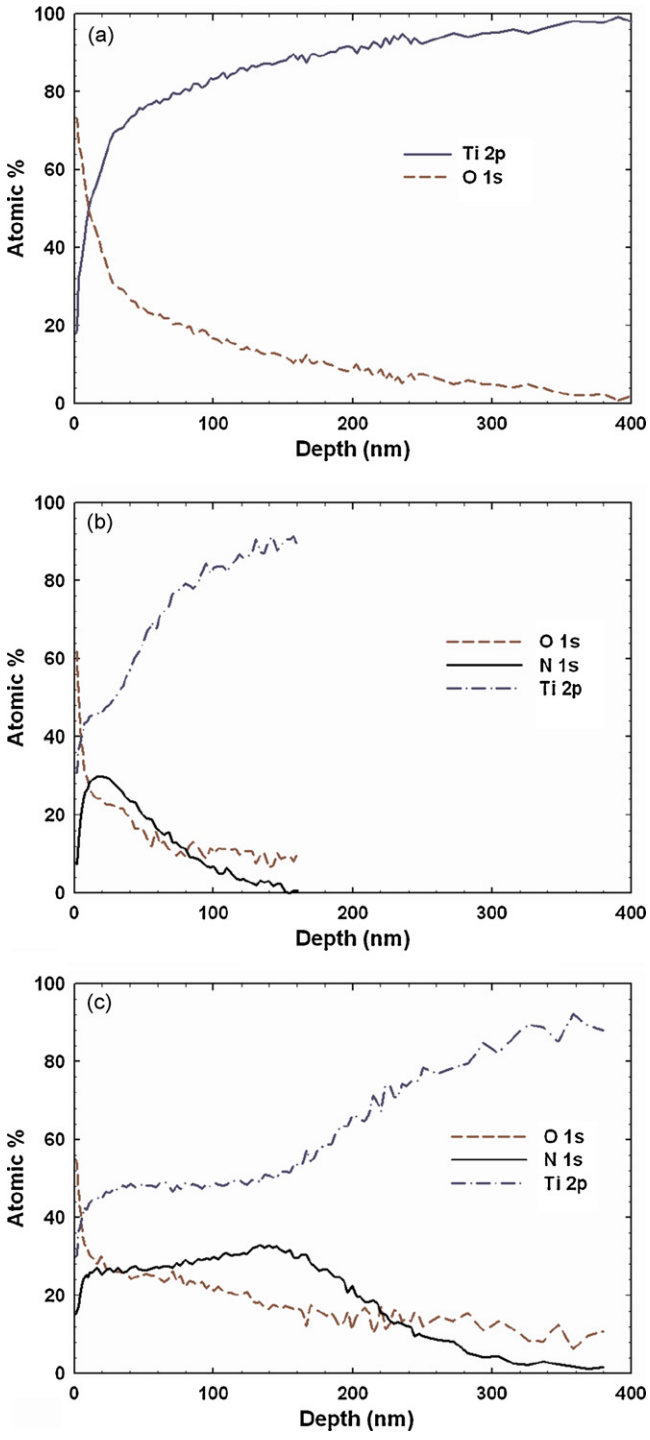

Fig. 1. XPS depth profiles acquired from (a) bare titanium sheet and (b) LT-PIII titanium, and (c) HT-PIII titanium.

Plasma immersion ion implantation (PIII) is a suitable technique to modify the surface of titanium [28,29]. This non-line-of-sight technique, which can effectively treat specimens with complex geometry such as a bipolar plate, boasts high efficiency, low cost, and environmentally friendliness as only nitrogen is used in the plasma [30]. The protective layer produced by PIII can effectively avoid the defects introduced by PVD as aforementioned. By choosing the proper duty cycle and controlling the sample cooling and heating rates, PIII can be conducted at a pre-designed temperature. In the present study, titanium sheets were treated by nitrogen PIII at both low and high temperature and the resulting effects on the corrosion resistance and conductivity were investigated systematically.

2. Experimental details

2.1. Materials and plasma immersion ion implantation nitriding

The temper annealed titanium sheets with a purity of 99.6% were purchased from Advent Research Materials Ltd. The sheets 1 mm thick were cut into 12 mm × 12 mm coupons for nitrogen plasma immersion ion implantation (PIII) and subsequent tests. The samples were polished with Nos. 600, 800, and 1200 SiC waterproof abrasive papers, cleaned with acetone and distilled water in an ultrasonic cleaner, and then dried in air. PIII was carried out in the Plasma Laboratory of City University of Hong Kong. The apparatus consisted of a stainless steel plasma discharge chamber (ϕ600 mm × 300 mm) and a stainless steel plasma diffusion chamber ((760 mm × 1030 mm). RF (radio frequency 13.56 MHz) power from 0 to 2 kW was coupled to the plasma discharge chamber. Negative high voltage pulses were applied to the metal sample stage through a ceramic high voltage feedthrough underneath the plasma diffusion chamber. The sample stage was a steel cylindrical sample stage 55 mm high and 160 mm in diameter supported by a metal rod with a diameter of 10 mm.

To conduct low-temperature PIII (LT-PIII), the high voltage sample stage and supporting voltage feedthrough were shielded from the plasma by a grounded metal tube 380 mm in diameter and 350 mm high. The metal tube was made of 2 mm thick aluminum and covered by a plate made of 2 mm thick stainless steel. A 150 mm diameter hole was opened at the center of the stainless steel plate. The hole was shielded by a stainless steel mesh with a line thickness of 0.6 mm having 12 lines per inch. The distance between the sample and cover was around 120 mm. Negative voltage pulses (−40 kV) were applied to the sample stage. Nitrogen gas was supplied to the chamber at a flow rate of 40.0 sccm to an operating pressure of 2 mTorr. After PIII, the temperature of the sample was measured to be below 100 °C.

High-temperature PIII (HT-PIII) was carried out without shielding the metal cage and so the sample was exposed directly to the nitrogen plasma. Nitrogen gas was bled into the vacuum cham-

ber at a flow rate of 20.0 sccm to a working pressure of 1 mTorr. 1000 W radio frequency power was matched to the plasma discharge chamber to generate the nitrogen plasma. Negative voltage pulses (−50 kV) were applied to the sample stage during the HT-PIII treatment which lasted 2 h. After PIII, the sample stage temperature was measured to be 370 °C by means of an infrared detector.

2.2. XPS analysis

The Ti, O and N profiles in the near surface region of the titanium sheets before and after PIII were acquired by X-ray photoelectron spectroscopy (XPS) on a Physical Electronics PHI 5802 equipped with a monochromatic Al K_α source. The peaks monitored in the depth profiles were Ti 2p, N 1s, and O 1s. The surface chemical composition and depth profiles were determined by using a constant pass energy of 11.75 eV and the photoelectrons were collected at a take-off angle of 45° with a step size of 0.25 eV.

2.3. Electrochemical and leaching tests

The samples for electrochemical measurements were embedded in epoxy resin to only expose a surface are of 10 mm × 10 mm and the backside of the sample was connected to a copper wire by soldering. The potentiodynamic and potentiostatic tests were conducted to evaluate the electrochemical behavior of the untreated and N-PIII titanium samples. A Zahner Zennium Electrochemical Workstation connected to a computer was used in the electrochemical experiments. A conventional three-electrode system in which the platinum sheet was the counter electrode, the saturated calomel electrode (SCE) worked as the reference electrode, and the sample served as the working electrode was adopted. Unless otherwise specified, all the electrode potentials were referenced to SCE. The electrochemical measurements were conducted in a 0.5 M H_2SO_4 solution with 2 ppm HF at 80 °C to accelerate the corrosion process in the simulated PEMFC environment. The solution was purged thoroughly with either hydrogen gas (to simulate the anode environment) or air (to simulate the cathode environment) prior to and during the electrochemical test. The relationship between the open circuit potential (OCP) and time was monitored for 1 h before the potentiodynamic polarization behavior was determined using a potential scanning rate of 1 mV s^{-1}. The potentiostatic test was performed to investigate the corrosion rate and stability of the control and N-PIII samples in the simulated PEMFC environment. It was conducted for 10 h at a potential of −0.1 V bubbled with H_2 and 0.6 V with air to simulate the anodic and cathodic operating environments in the PEMFC, respectively. Afterwards, the solutions (about 100 ml) were collected and analyzed by inductively coupled plasma optical emission spectrometry (ICP-OES) OPTIMA 2100 DV to determine the amounts of dissolved Ti.

2.4. Interfacial contact resistance (ICR)

The interfacial contact resistance (ICR) of the untreated titanium, LT N-PIII, and HT N-PIII samples were measured by the

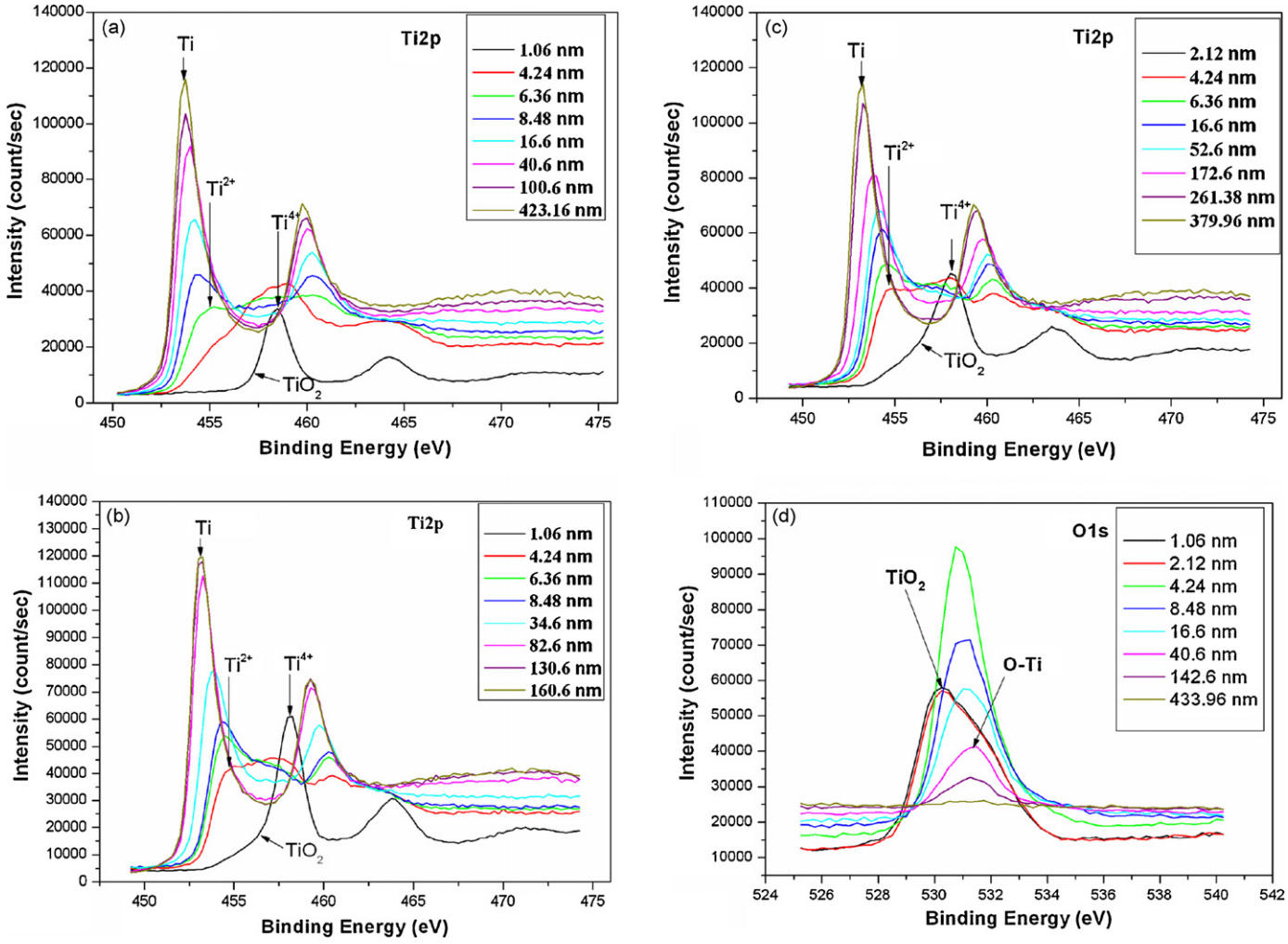

Fig. 2. Ti 2p, O 1s and N 1s XPS spectra as a function of sputtering depths (nm) acquired from: (a and d) bare Ti, (b, e, and g) LT-PIII sample, and (c, f, and h) HT-PIII titanium.

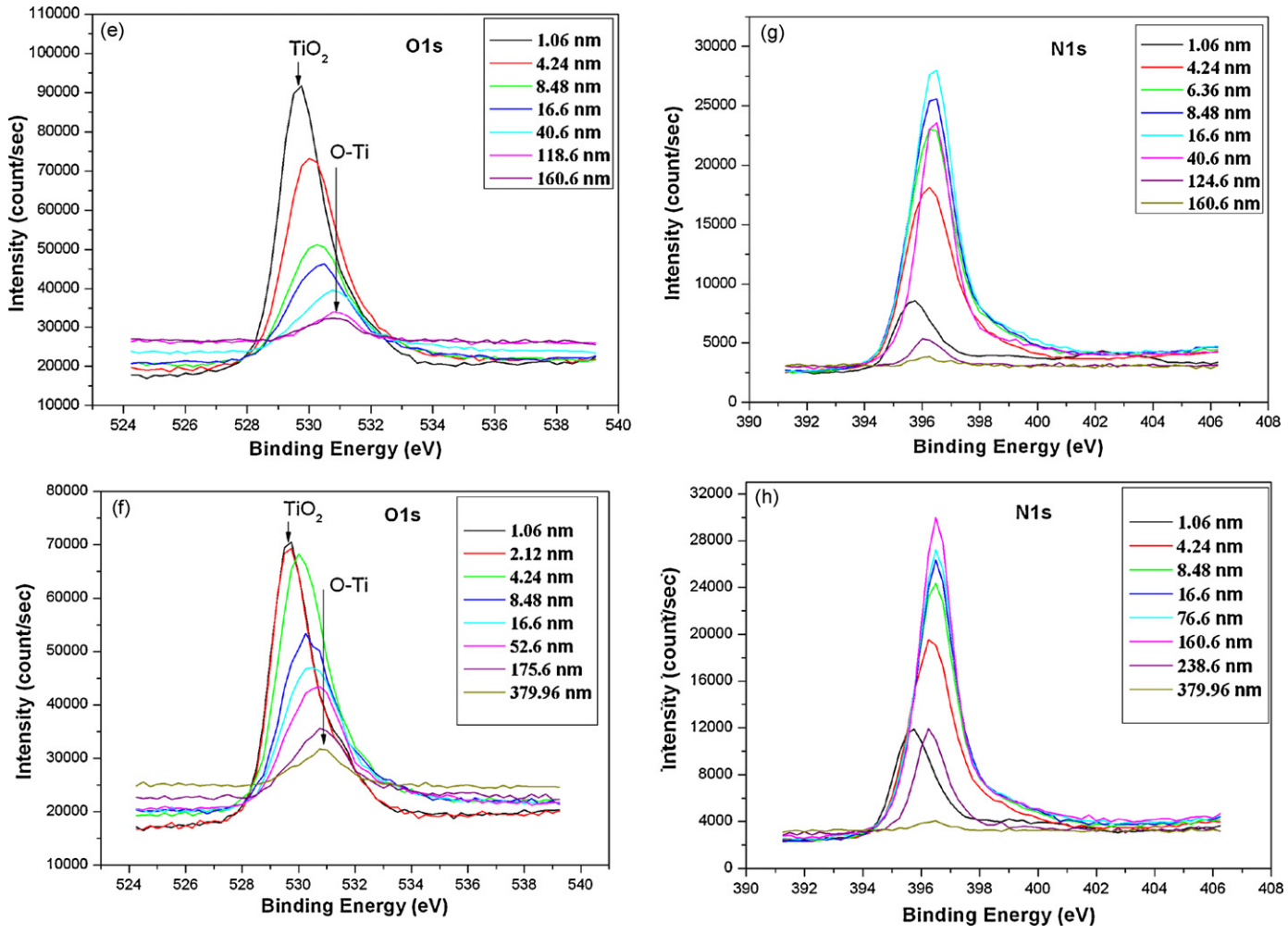

Fig. 2. (*Continued*).

method proposed by Davies et al. [31] and improved by Wang et al. [32]. The sample was enclosed by two pieces of conductive carbon paper (Toray TGP-H-090) that were sandwiched between the sample and two copper plates. A constant current (0.1 A) was applied via the two copper plates, and the variation in the total voltage was recorded with respect to the compaction force that was steadily increased. More details about this method can be found in the literature [32].

3. Results and discussion

3.1. XPS analysis

The XPS depth profiles acquired from the bare and PIII titanium samples are depicted in Fig. 1. The profiles are plotted on a depth scale based on sputtering rates calculated from a SiO_2 reference under similar conditions. Since it is known that the sputtering rate of titanium is different from that of SiO_2, the thickness is approximate, but comparison among different samples is more valid. The nitrogen depth profile in the LT-PIII titanium is narrower compared to that of the HT-PIII sample. The higher implantation temperature spurs substantial nitrogen diffusion resulting in a broader nitrogen profile that has a concentration of about 25 at.% in the depth range between 10 and 200 nm from the surface. The oxygen concentration close to the outer surface does not differ much from the value of about 60 at.% obtained from the untreated titanium as well as the LT and HT N-PIII samples. However, the HT-PIII sample has a higher oxygen concentration (about 25 at.%) which decreases slowly with depths and it may be due to the higher temperature and oxygen diffusion as observed from Fig. 1(c).

In order to investigate the changes in the Ti 2p, O 1s and N 1s chemical states, high resolution XPS spectra are taken at different sputtered depths and the results are displayed in Fig. 2. The montages, which illustrate the changes in the XPS peak shape and position at different depths, show that the titanium samples before and after nitrogen PIII are covered by a surface layer of TiO_2. At a depth of about 4–5 nm, the valence state of titanium in the nitrogen PIII sample starts to change from Ti^{4+} to Ti^{2+}, whereas this change occurs at 6–7 nm in the untreated one. As shown in Fig. 2(d)–(f), titanium oxynitride is formed since O–Ti can be detected from both the LT-PIII and HT-PIII samples. Fig. 2(g) and (h) shows the XPS spectra of the N implanted titanium sheet. The peak at the lower binding energy corresponds to Ti–O whereas the peak at a higher binding energy at around 397 eV is associated with the N–Ti–O bond. It can be observed that in the HT-PIII sample, the implanted nitrogen depth is larger and the region (depth) showing the N–Ti–O bond is broader.

3.2. Electrochemical results

The potentiodynamic polarization curves measured from the bare, LT-PIII, and HT-PIII samples in the 0.5 M H_2SO_4 solution with 2 ppm HF at 80 °C are displayed in Fig. 3. The corrosion potential (E_{corr}), corrosion current density (I_{corr}), and current density at

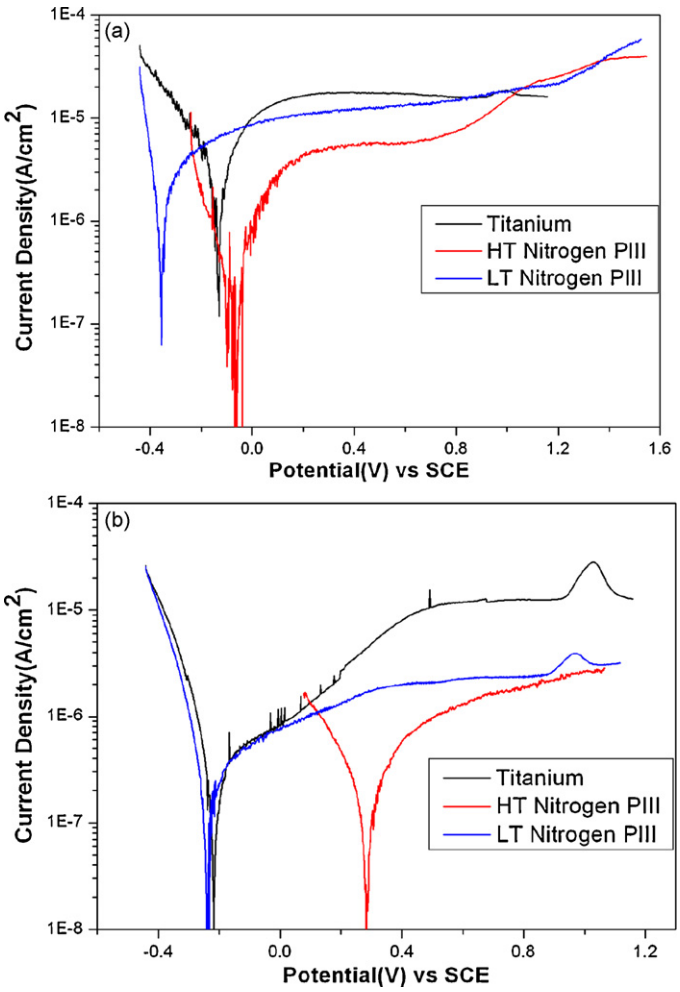

Fig. 3. Polarization curves obtained from the bare as well as LT-PIII and HT-PIII titanium sample in a 0.5 M H_2SO_4 solution with 2 ppm HF at 80 °C: (a) aspirated with H_2 and (b) aspirated with air.

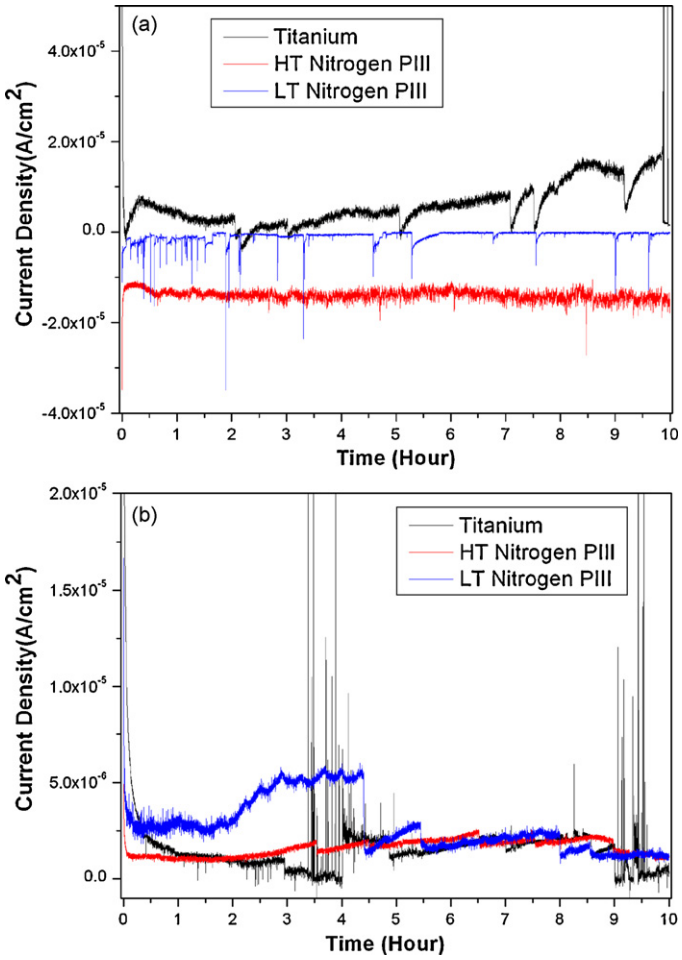

Fig. 4. Potentiostatic curves of the bare as well as LT-PIII and HT-PIII titanium sample in: (a) simulated anode (−0.1 V vs. SCE aspirated with H_2) and (b) cathode environment (0.6 V vs. SCE aspirated with air).

the operating potential in both the anodic and cathodic environments (I_w) are summarized in Table 1. In general, the titanium samples before and after nitrogen PIII have a passive region. In the anodic environment, the corrosion potential of titanium shifts towards the positive direction from −134 to −70 mV after HT-PIII, but that drops to −357 mV after LT-PIII. However, the corrosion current density of titanium decreases after both LT-PIII and HT-PIII. Since the anodic operating potential in the PEMFC is about −0.1 V, a current density at −0.1 V is also indicated. The bare and LT-PIII samples show anodic dissolution and the current densities are 3.0 and 5.7 μA cm^{-2}, respectively. The current density of the HT-PIII sample at the anodic operating potential is −0.2 μA cm^{-2}, indicating cathodic protection by the titanium oxy-nitride layer formed at higher temperature. Fig. 3(b) shows the potentiodynamic polarization results when the solution is purged with air to simulate the cathodic environment in the PEMFC environment. It can be observed that the cathodic operating potential (0.6 V) is in the passive region in all the samples. The corrosion potential of the LT-PIII sample is similar to that of bare titanium but the current density in the passive region is much lower. After HT-PIII, the corrosion resistance is significantly improved. The corrosion potential is 282 mV, corrosion current density is 0.06 μA cm^{-2}, and current density at the cathodic operating potential is 1.3 μA cm^{-2}.

In the PEMFC, the anodic and cathodic conditions are −0.1 V vs. SCE (purged with H_2) and 0.6 V vs. SCE (purged with air), respectively. Therefore, the bipolar plates undergo corrosion at an applied potential which is different from the free corrosion potential and the potentiostatic test should be carried out to assess corrosion in both the simulated PEMFC anodic and cathodic environments. The current density as a function of time is plotted in Fig. 4. Fig. 4(a) presents the potentiostatic curves at −0.1 V vs. SCE obtained from the bare, LT-PIII, and HT-PIII titanium samples in the anodic environment. The current density in the bare titanium decays very fast initially, undergoes a negative–positive switch, and then a positive–negative switch gradually stabilizing

Table 1
Polarization parameters of the bare Ti, LT-PIII Ti, and HT-PIII-N Ti samples in 0.5 M H_2SO_4 + 2 ppm HF solution at 80 °C.

	Anode environment			Cathode environment		
	E_{corr} (mV)	I_{corr} (μA cm^{-2})	I_w (μA cm^{-2})	E_{corr} (mV)	I_{corr} (μA cm^{-2})	I_w (μA cm^{-2})
The bare titanium	−134	1.45	3.0	−218	0.16	11.9
HT-PIII titanium	−70	0.22	−0.2	−235	0.07	1.3
LT-PIII titanium	−357	0.86	5.7	282	0.06	2.3

Table 2
Ti ion concentrations leached from the bare Ti, LT-PIII Ti, and HT-PIII Ti samples after 10 h potentiostatic tests (averages of two samples).

Sample	PEMFC anode environment (ppb)	PEMFC cathode environment (ppb)
Titanium	4864.45	121.45
HT nitrogen PIII	155.08	112.00
LT nitrogen PIII	360.83	309.15

at a relatively higher current density. The dramatic change in the current density is possibly related to the formation of the passive film. As soon as the entire surface is covered by the passive film, the current density required to maintain passivation is more stable. During the process, the current density undergoes several sharp drops which are due to the unstable passive film formed on titanium in the simulated PEMFC environment. As for the LT-PIII and HT-PIII samples, the current density is cathodic, indicating that the samples are cathodically protected and the active dissolution rate is low in the simulated anodic environment. However, the current density in the LT-PIII sample exhibits sharp changes during polarization. Fig. 4(b) shows the potentiostatic curves at 0.6 V vs. SCE in the simulated PEMFC cathodic environment. The current density in all the samples decreases rapidly in the beginning then gradually stabilizes reflecting the formation of a passive film on the surface. However, the current density on the bare titanium is not stable during the experiment. In comparison, the current density measured from the HT-PIII sample is quite stable and low ranging between 1.0 and 1.6 $\mu A\,cm^{-2}$ throughout the experiment.

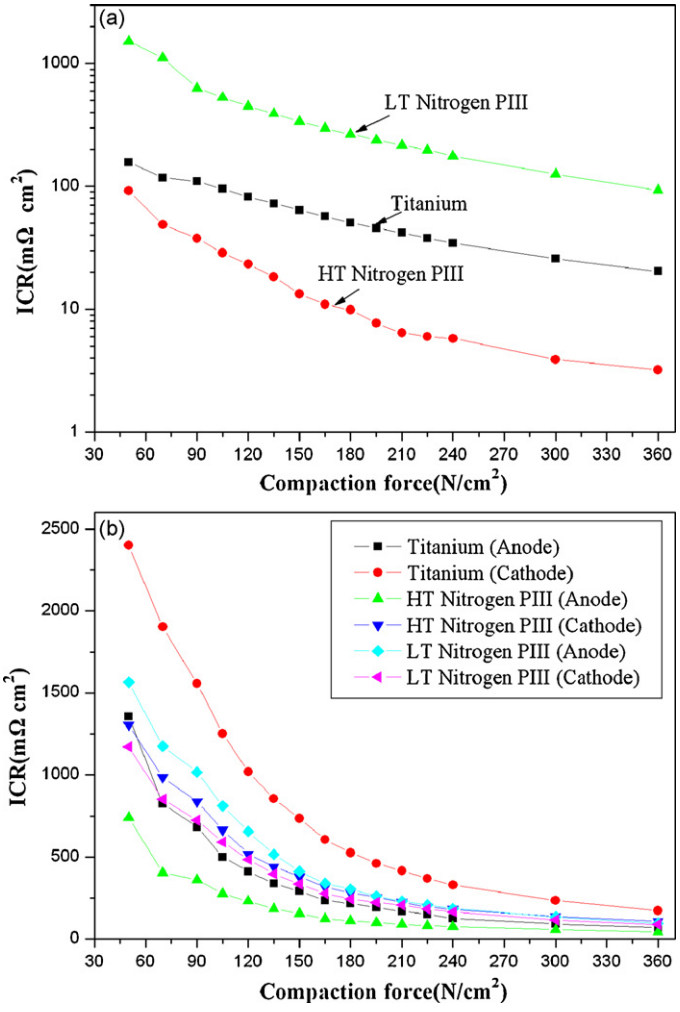

Fig. 5. (a) Variations in the interfacial contact resistance (ICR) values obtained on the bare Ti, LT-PIII Ti, and HT-PIII Ti and (b) values obtained after the potentiostatic test in the anode and cathode PEMFC environments.

3.3. ICP measurements

In the real PEMFC environment, the metal ions corroded from the bipolar plate may migrate to the electrodes and poison the electro-catalysts via the electrodes and ion exchange with the proton groups in the solid polymer electrolyte. The metal ions generated during corrosion in the solution constitute a very important parameter to gauge the performance of the bipolar plates. Therefore, the solutions after the potentiostatic test for 10 h are collected and the metal ions dissolved are determined by inductively coupled plasma optical emission spectroscopy. As shown in Table 2, the bare titanium suffers from serious corrosion in the simulated PEMFC anodic environment and the Ti ion concentration is 121 ppb. The obvious difference between the anodic and cathodic environments arises from that titanium has good corrosion resistance at high positive overpotentials [25]. After HT-PIII, the Ti concentrations are reduced to 155 ppb in the anode environment and 112 ppb in the cathode environment. The ion concentration leached from the LT-PIII sample is higher than that from the HT-PIII sample in both the anodic and cathodic environments. These results imply that good corrosion resistance is achieved by HT nitrogen PIII treatment and it is in good agreement with the electrochemical test results (Figs. 3 and 4).

3.4. Interfacial contact resistance (ICR)

The interfacial contact resistance (ICR) values determined from the bare, LT-PIII, and HT-PIII titanium and after the potentiostatic test in the anode and cathode PEMFC environments samples are plotted as a function of compaction force in Fig. 5. The ICR values decrease with increasing compaction force due to the increasing effective contact areas between the carbon paper and samples. However, when the compaction force is increased to a certain value, there is no apparent change in the ICR because the effective contact area reaches the limit. As shown in Fig. 5(a), the ICR determined from the HT-PIII titanium is lower than that from the bare titanium throughout the entire range of applied compaction force. In particular, the ICR value of the HT-PIII titanium is 23.2–6.4 $m\Omega\,cm^2$ under 120–210 $N\,cm^{-2}$, and that of bare titanium is 82.1–41.8 $m\Omega\,cm^2$ under the same compaction force. Compared to the bare titanium sheet, the LT-PIII sample has much higher ICR values. At compaction force ranging from 120 to 210 $N\,cm^{-2}$, the ICR values vary between 449.3 and 216.7 $m\Omega\,cm^2$. The results indicate that the surface titanium oxy-nitride layer formed by HT nitrogen PIII is highly conductive but that formed at low temperature is less conductive. When the temperature during PIII is high, oxygen atoms diffuse faster and can more readily move to the grain boundaries. This effect is believed to increase the electrical conductivity and prevent the corrosive media from penetrating the substrate [24]. Fig. 5(b) shows that the ICR values of all the samples increase after the potentiostatic test in both the anode and cathode environments. It is reasonable that the ICR value after the potentiostatic test in the anode environment is lower than that in the cathode environment since the passive film is more difficult to form in the anode environment due to the presence of hydrogen. The results acquired from the bare titanium and HT-PIII titanium confirm it. In fact, the sample, HT nitrogen PIII (anode), has the lowest ICR among the samples, followed by titanium (anode). In contrary, the LT-PIII sample does not exhibit this characteristic.

4. Conclusion

Titanium sheets are subjected to low-temperature and high-temperature nitrogen plasma immersion ion implantation (LT-PIII and HT-PIII). XPS discloses that titanium oxy-nitride layers are formed in the Ti samples after PIII. The HT-PIII titanium sample has a thicker modified layer than the LT-PIII sample. The electrochemical and ICP results indicate that the corrosion resistance of Ti is significantly improved after HT-III but the enhancement after LT-PIII is not as significant. The ICR results reveal that an oxy-nitride layer with high electrical conductivity is formed by HT-PIII but the conductivity of the LT-PIII sample is poorer. After the potentiostatic test, the ICR values of all the samples increase due to the formation of passive films. At a high temperature, oxygen atoms diffuse to the grain boundaries consequently increasing the corrosion resistance and conductivity. Our results suggest that high-temperature nitrogen plasma immersion ion implantation can significantly improve the corrosion resistance and conductivity of titanium in the simulated PEMFC environment.

Acknowledgements

Financial support provided by National Natural Science Foundation of China under contract number 50820125506 and Hong Kong Research Grants Council (RGC) General Research Funds (GRF) No. CityU 112608 is acknowledged.

References

[1] B.L. Yi, Fuel Cell-Theory Technology Application, 1st ed., Chemical Industry Press, Beijing, 2003, pp. 160–161.
[2] T. Fukutsuka, T. Yamaguchi, S.I. Miyano, Y. Matsuo, Y. Sugie, Z. Ogumi, J. Power Sources 174 (2007) 199–205.
[3] J. Marcinkoski, J.P. Kopasz, T.G. Benjamin, Int. J. Hydrogen Energy 33 (2008) 3894–3902.
[4] R.F. Silva, D. Franchi, A. Leone, L. Pilloni, A. Masci, A. Pozio, Electrochim. Acta 51 (2006) 3592–3598.
[5] V. Mehta, J.S. Cooper, J. Power Sources 114 (2003) 32–53.
[6] M. Li, S. Luo, C. Zeng, J. Shen, H. Lin, C. Cao, Corros. Sci. 46 (2004) 1369–1380.
[7] M. Kumagai, S.T. Myung, S. Kuwata, R. Asaishi, H. Yashiro, Electrochim. Acta 53 (2008) 4205–4212.
[8] A. Hermann, T. Chaudhuri, P. Spagnol, Int. J. Hydrogen Energy 30 (2005) 1297–1302.
[9] R. Tian, J. Sun, J. Wang, Int. J. Hydrogen Energy 33 (2008) 7507–7512.
[10] H. Wang, J.A. Turner, J. Power Sources 128 (2004) 193–200.
[11] V.V. Nikam, R.G. Reddy, Int. J. Hydrogen Energy 31 (2006) 1863–1873.
[12] J. Liu, F. Chen, Y. Chen, D. Zhang, J. Power Sources 187 (2009) 500–504.
[13] S. Joseph, J.C. McClure, R. Chianelli, P. Pich, P.J. Sebastian, Int. J. Hydrogen Energy 30 (2005) 1339–1344.
[14] A. Kumara, R.G. Reddy, J. Power Sources 129 (2004) 62–67.
[15] K. Feng, Y. Shen, H. Sun, D. Liu, Q. An, X. Cai, P.K. Chu, Int. J. Hydrogen Energy 34 (2009) 6771–6777.
[16] M.P. Brady, H. Wang, B. Yang, J.A. Turner, M. Bordignon, R. Molins, M. Abd Elhamid, L. Lipp, L.R. Walker, Int. J. Hydrogen Energy 32 (2007) 3778–3788.
[17] R.F. Silva, A. Pozio, J. Fuel Cell Sci. Technol. 4 (2007) 116–122.
[18] Y. Show, M. Miki, T. Nakamura, Diamond Relat. Mater. 16 (2007) 1159–1161.
[19] Y. Wang, D.O. Northwood, Int. J. Hydrogen Energy 32 (2007) 895–902.
[20] K.H. Cho, W.G. Lee, S.B. Lee, H. Jang, J. Power Sources 178 (2008) 671–676.
[21] Y. Wang, D.O. Northwood, J. Power Sources 165 (2007) 293–298.
[22] B. Elsener, A. Rota, H. Böhni, Mater. Sci. Forum 44 (1989) 29–38.
[23] D. Yang, C. Liu, X. Liu, M. Qi, G. Lin, Curr. Appl. Phys. 5 (2005) 417–421.
[24] S.Y. Kim, D.H. Han, J.N. Kim, J.J. Lee, J. Power Sources 193 (2009) 570–574.
[25] H.Y. Jung, S.Y. Huang, P. Ganesan, B.N. Popov, J. Power Sources 194 (2009) 972–975.
[26] D.R. Hodgson, B. May, P.L. Adcock, D.P. Davies, J. Power Sources 96 (2001) 233–235.
[27] S.H. Wang, J. Peng, W.B. Lui, J. Power Sources 160 (2006) 485–489.
[28] P.K. Chu, S. Qin, C. Chan, N.W. Cheung, L.A. Larson, Mater. Sci. Eng. Rep. 17 (1996) 207–280.
[29] P.K. Chu, J.Y. Chen, L.P. Wang, N. Huang, Mater. Sci. Eng. Rep. 36 (2002) 143–206.
[30] R.W.Y. Poon, J.P.Y. Ho, X.Y. Liu, C.Y. Chung, P.K. Chu, K.W.K. Yeung, W.W. Lu, K.M.C. Cheung, Thin Solid Film 488 (2005) 20–25.
[31] D.P. Davies, P.L. Adcock, M. Turpin, S.J. Rowen, J. Power sources 86 (2000) 237–242.
[32] H. Wang, M.A. Sweikart, J.A. Turner, J. Power sources 115 (2003) 243–251.